

Oxyanion Inhibition of Passivity Breakdown and the Nucleation of Pits on Type 316L Stainless Steel

Digby D. Macdonald and Shoufeng Yang
Center for Electrochemical Science and Technology
Department of Materials Science and Engineering
Pennsylvania State University
201 Steidle Bldg
University Park, PA 16802

ABSTRACT

Passivity breakdown of Type 316L SS (UNS S31603) in the presence of aggressive Cl^- and inhibitive NO_3^- anions has been experimentally studied and the results have been interpreted in terms of the Point Defect Model (PDM). By expanding the PDM to include competitive adsorption of Cl^- and NO_3^- into surface oxygen vacancies at the passive film/solution interface, the critical breakdown potential (V_c) has been predicted to vary linearly with $\log[\text{Cl}^-]$ and with $\log\left(\frac{[\text{Cl}^-]}{[\text{NO}_3^-]}\right)$, which is found experimentally. The slope of V_c vs. $\log[\text{Cl}^-]$ is found to be unaffected by NO_3^- , thereby yielding the same values for the polarizability of the film/solution interface, regardless of the nitrate concentration. The critical breakdown potential increases weakly with increasing nitrate concentration at low $[\text{NO}_3^-]$ but, at a concentration of 0.06 M, V_c increases sharply and pitting attack is no longer observed. The viability of the PDM for accounting for passivity breakdown on Type 316 SS is explored by measuring the voltage scan rate dependence of the critical breakdown potential, from which the critical areal (two dimensional) concentration of condensed vacancies at the metal/barrier layer interface can be derived. Good agreement between the value obtained from experiment and those calculated from structural arguments demonstrate the validity of the PDM.

Key Words: Passivity breakdown, oxyanion inhibition, Type 316L SS, Point Defect Model.

INTRODUCTION

Passivity breakdown is the precursor to the development of all localized corrosion events on metal and alloy surfaces in contact with aggressive aqueous solutions. While the processes involved are reasonably well understood,^{1,2} the observation that certain species inhibit passivity breakdown remains to be fully accounted for theoretically. Briefly, the experimental evidence is that certain oxyanions, such as nitrite (NO_2^-), nitrate (NO_3^-), chromate (CrO_4^{2-}), and sulfate (SO_4^{2-}), inhibit the ability of chloride ion (for example) to nucleate pits upon a metal surface (e.g., Fe) by displacing the critical pitting potential in the positive direction and by increasing the induction time at a constant potential.³⁻⁸ The critical pitting potential is found to take the form³

$$E_{\text{pit}} = E_{\text{pit}}^0 - B \log \left(\frac{[\text{Cl}^-]}{[\text{A}^{z-}]} \right) \quad (1)$$

where E_{pit}^0 is a constant (equal to the pitting potential when $[\text{Cl}^-]/[\text{A}^{z-}] = 1$), B is a constant that generally has a value that is greater than $2.303RT/F$ and A^{z-} represents the inhibiting oxyanion.

The purpose of this paper is to extend the Point Defect Model (PDM)^{1,2} to account for the inhibition of passivity breakdown by oxyanion species. The model assumes competitive adsorption of the aggressive and inhibiting species into surface oxygen vacancies, with the adsorption of X^- culminating in the autocatalytic generation of cation vacancies at the barrier layer/solution interface and their subsequent condensation at the metal barrier layer interface.^{1,2} The theory successfully accounts for the form of Equation (1) and it provides clear guidance as to the selection of the most effective inhibitors. Finally, the extended PDM is readily inserted into the pit nucleation function of Damage Function Analysis (DFA),⁹ in order to incorporate oxyanion inhibition into the deterministic prediction of localized corrosion damage.

PASSIVITY BREAKDOWN

According to the existing Point Defect Model,^{1,2} passivity breakdown results from the condensation of cation or metal vacancies at the metal/barrier layer interface under conditions where the vacancy flux is sufficiently high, due to the aggressive anion-induced, autocatalytic generation of cation vacancies at the barrier layer/solution interface, that all of the vacancies cannot be annihilated at the metal/barrier layer interface by Reaction (1), Figure 1. The excess vacancies then condense to form a two-dimensional vacancy condensate beneath the “weak points” in the barrier layer that are characterized by high cation vacancy diffusivity. Vacancy condensation effectively causes local separation between the barrier layer and the metal, as depicted in the cartoon, Figure 2. However, the film keeps growing into the metal at those points where separation has not occurred and the barrier layer keeps dissolving at the film/solution interface and hence the film thins over the condensate. At some point in time, the “cap” over the condensate will become so thin that it will fracture under the growth stresses

that exist in the film, marking a breakdown event (Figure 2). The nucleus may repassivate promptly, due to failure to establish a differential aeration cell (DAC) (“prompt repassivation”), marking a meta stable event, or may establish a viable DAC resulting in the growth of a macroscopic pit. The survival probability of a stable pit is defined as $SP = 1/(1+N)$, where N is the number of metastable events that occur before the formation of a stable pit. The value of SP is typically 10^{-2} to 10^{-5} , depending upon the material and the environmental conditions.

This mechanistic picture now needs to be modified as the result of closer examination of experimental data that were not available when the PDM was originally synthesized.^{1,2} Briefly, condensation is now considered to be possible on either the cation sublattice of the film or on the metal lattice at the interface, with the two locations being related through the reaction, $m + V_M^{\chi'} \xrightarrow{k_1} M_M + v_m + \chi e'$, where $V_M^{\chi'}$ is a vacancy on the cation sublattice of the barrier layer at the film side of the barrier layer/metal interface and v_m is a vacancy on the metal lattice on the metal side of that same interface. Additionally, other processes that generate v_m must be considered, as discussed in greater detail below. Suffice it to state at this point that annihilation of the vacancy on the metal lattice can occur via a number of processes, including diffusion to a free interface (or grain boundary) and dislocation climb. In any event, the two-dimensional vacancy condensate continues to grow via vacancy condensation at the periphery. Because the film continues to dissolve at the barrier layer/solution interface, the cap over the condensate gradually thins and, at some point, rupture occurs, thereby marking a breakdown event. If the nucleus dies immediately (within milliseconds to seconds), because of prompt repassivation, the event is labeled a “metastable pit”. However, as noted above, a small fraction of the breakdown events survive and establish viable micro cells having the appropriate separation between the local anode (in the pit nucleus) and the local cathode (on the external surface), thereby resulting in the growth of stable pits.

With reference to Figure 2, it is evident that the induction time for passivity breakdown comprises two components: (1) That required for the condensation of sufficient vacancies at the metal/barrier layer interface to cause separation of the barrier layer from the metal, and hence to stop the growth of the barrier layer into the substrate via Reaction (3), Figure 1, and; (2) the time for dissolution of the “cap” (remnant of the barrier layer) over the breakdown site to the point that fracture occurs. The general condition is given by Equation (2):

$$(J_{CA} - J_m)(t - \tau) \geq \xi \quad (2)$$

where J_{CA} and J_m are the rates of generation and annihilation, respectively, of cation vacancies at the metal/barrier layer interface, t is time, and τ the time of dissolution of the cap. For steady state dissolution, this latter quantity becomes

$$\tau \leq \Omega_{ss}^{VC} / k_7 (C_{H^+} / C_{H^+}^0)^n \quad (3)$$

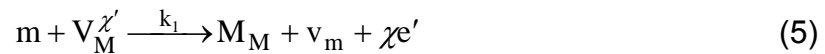
In this expression, Ω is the mole volume of the barrier layer per gram cation, L_{ss}^{VC} is the thickness of the barrier layer at the point of initial vacancy condensation, k_7 is the rate constant for the barrier layer dissolution reaction, C_{H^+} is the concentration of hydrogen ion at the barrier layer/solution interface, and $C_{H^+}^0$ is a standard state hydrogen ion concentration (included to insure that the units of the rate constant, k_7 , are independent of the reaction order, n).

It is evident from Equation (2) that the critical condition for passivity breakdown at a specific site occurs when $t \rightarrow \infty$ or when

$$J_{CA} \rightarrow J_m \quad (4)$$

This condition results in an expression for the critical breakdown potential for a single site, regardless of the fate of the nucleus (i.e., irrespective of whether the breakdown event results in a metastable or stable pit).^{1,2} Derivation of an expression for the critical breakdown potential, V_c , is obtained as the solution to Equation (2), as described below. The processes that are envisioned to lead to the enhanced flux of cation vacancies across the barrier layer from the film/solution interface to the metal/film interface upon the absorption of the aggressive anion into surface oxygen vacancies are depicted in Figure 3. Two basic mechanisms are envisioned for the generation of cation vacancies at the film/solution interface; a Schottky pair reaction and ion desorption/vacancy pair generation. Both processes are autocatalytic in the oxygen vacancy, in that the oxygen vacancies are regenerated at the periphery of the vacancy condensate and hence are available to absorb additional aggressive anion. This is an important feature of the mechanism, because it explains the observation of Barger and Givens [10,11] that chloride ion redistributes to the periphery of the blister on aluminum that is the site of passivity breakdown and it accounts for the fact that the breakdown process does not “saturate”, as might be expected for static absorption.

The process of vacancy annihilation/condensation at the metal/barrier layer interface has not received in-depth examination. In essence, there are two possibilities that may be identified; (1) Condensation of cation vacancies, $V_M^{\chi'}$, on the cation sublattice of the barrier layer adjacent to the interface; and (2) Condensation of metal vacancies, v_m , on the metal lattice on the substrate side of the interface. Both are envisioned to involve at least Reaction (1), Figure 1



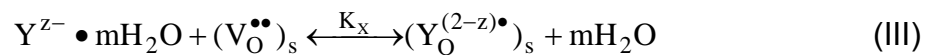
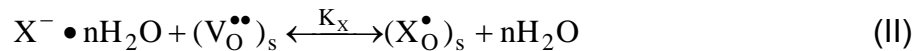
In the first scenario, those cation vacancies of the enhanced flux across the film that cannot be annihilated by Reaction (5) are envisioned to condense at the periphery of a two-dimensional condensate, thereby effectively separating the barrier layer from the substrate metal and preventing further growth of the barrier layer into the metal, as discussed above. In the second scenario, the vacancies that are generated on the metal lattice by Reaction (5) and/or other processes (see below), v_m , are annihilated by

processes that occur on the metal side of the metal/barrier layer interface, such as dislocation climb or diffusion to a free interface, as might exist, for example, at a free surface or at a void or grain boundary. For metals and alloys that form p-type semi-conducting barrier layers, such as nickel,¹ in which cation vacancies are the principal point defect, Reaction (5) is postulated to be the primary source of vacancies on the metal lattice at the metal/barrier layer interface. However, metals and alloys that display n-type electronic character (e.g., Fe, Zn, stainless steel),¹ also suffer passivity breakdown, so that the annihilation of cation vacancies alone via Reaction (5) might not be the sole source of v_m , in the general case. The other source, of course, is Reaction (2), Figure 1; the generation of cation interstitials



Adsorption of Solution-Phase Species into Surface Oxygen Vacancies

Competitive adsorption has been invoked previously as a mechanism for the inhibition of pitting corrosion by oxyanions,³⁻⁸ but to the authors' knowledge it has not previously been used in conjunction with cation vacancy generation at the metal/film interface to account for the experimental findings. In general terms, it is necessary to consider the absorption of three adsorbates into surface oxygen vacancies; H₂O resulting in the injection of oxygen ions into the barrier layer, the aggressive anion, X⁻, resulting in cation vacancy generation (see below), and the inhibiting species, Y^{z-}, which effectively competes with X⁻ for the available oxygen vacancies. The equilibria involved are written as



where $(O_O)_s$, $(X_O^\bullet)_s$, and $(Y_O^{(2-z)\bullet})_s$ are the absorbed species, as expressed in Kroger-Vink notation, and $(V_O^{\bullet\bullet})_s$ represents a surface oxygen vacancy. Note that partial dehydration of the anions, at least, must occur during the absorption process.

Let Γ^0 be the surface concentration of anion sublattice sites on the barrier layer surface (mol/cm²). Thus,

$$\Gamma^0 = \Gamma_{V_o} + \Gamma_{O_o} + \Gamma_{X_o} + \Gamma_{Y_o} \quad (7)$$

where Γ_{V_o} , Γ_{O_o} , Γ_{X_o} , and Γ_{Y_o} are the surface concentrations of oxygen vacancies, oxide ions, adsorbed X^- , and adsorbed Y^{2-} , respectively. The equilibrium conditions for Reactions (I) to (III) may be stated by equating the electrochemical potentials

$$\tilde{\mu} = \mu^0 + RT \ln(a) + zF\phi \quad (8)$$

of both sides, where μ^0 is the standard chemical potential, a is the activity, z is the species charge (including sign), and ϕ is the electrostatic potential at the point of interest. By noting that, according to the Point Defect Model,¹

$$\phi_{f/s} = \phi_f - \phi_s = \alpha V + \beta pH + \phi_{f/s}^0 \quad (9)$$

where α is the polarizability of the film (barrier layer)/solution interface, β is the dependence of the potential drop across the barrier layer/solution interface ($\phi_{f/s}$) on pH, and $\phi_{f/s}^0$ is a constant, and by carefully identifying the location of each species with respect to the film (barrier layer)/solution (f/s) interface, and hence with respect to the local potential (ϕ_f or ϕ_s), the equilibrium constants may be written as

$$K_I = K_I^0 e^{\frac{2\alpha FV}{RT}} e^{\frac{2\beta FpH}{RT}} \quad (10)$$

$$K_{II} = K_{II}^0 e^{\frac{\alpha FV}{RT}} e^{\frac{\beta FpH}{RT}} \quad (11)$$

and

$$K_{III} = K_{III}^0 e^{\frac{z\alpha FV}{RT}} e^{\frac{z\beta FpH}{RT}} \quad (12)$$

where $K_I^0 = e^{-(\Delta\mu_I^0 - 2F\phi_{f/s}^0)/RT}$, $K_{II}^0 = e^{-(\Delta\mu_{II}^0 - F\phi_{f/s}^0)/RT}$, and $K_{III}^0 = e^{-(\Delta\mu_{III}^0 - zF\phi_{f/s}^0)/RT}$. The parameter $\Delta\mu_j^0$ is the change in standard Gibbs energy for the j^{th} absorption equilibrium [Reactions (I) to (III)]. Manipulation of these equations, together with the definitions of the equilibrium constants, $K_I = \Gamma_{O_o} a_{H^+}^2 / \Gamma_{V_o} a_{H_2O}$, $K_{II} = \Gamma_{X_o} / \Gamma_{V_o} a_X$, and $K_{III} = \Gamma_{Y_o} / \Gamma_{V_o} a_Y$, yields the concentrations of the surface species as follows:

$$\Gamma_{V_o} = \Gamma^0 \left\{ 1 + \frac{K_I^0 G_I}{a_{H^+}^2} + K_{II}^0 G_{II} a_X + K_{III}^0 G_{III} a_Y \right\} \quad (13)$$

$$\Gamma_{O_o} = K_I^0 G_I \Gamma_{V_o} / a_{H^+}^2 \quad (14)$$

$$\Gamma_{X_o} = K_{II}^0 G_{II} \Gamma_{V_o} a_X \quad (15)$$

$$\Gamma_{Y_o} = K_{III}^0 G_{III} \Gamma_{V_o} a_Y \quad (16)$$

where G_I , G_{II} , and G_{III} are defined as

$$G_I = e^{2F(\alpha V + \beta p H) / RT} \quad (17)$$

$$G_{II} = e^{F(\alpha V + \beta p H) / RT} \quad (18)$$

and

$$G_{III} = e^{zF(\alpha V + \beta p H) / RT} \quad (19)$$

The reader will note that in deriving these equations, we have assumed Langmuir absorption conditions: (1) No interaction exists between absorbed species; and (2) the absorption sites are identical. Non-ideality may be taken into account by considering the Γ values to be surface activities defines as $\Gamma_i = \hat{\gamma}(\zeta / \zeta^0)$, where $\hat{\gamma}$ is the activity coefficient (> 1 for attractive interactions and < 1 for repulsive interactions), ζ is the surface concentration in mol/m², and ζ^0 is the surface concentration in the standard state [sensibly chosen to be 1.0 μmol/m²]. Note that, for a typical oxide, there are about 2×10^{19} surface anion sites per square meter, which, when divided by Avogadro's number (6.023×10^{23} /mol), yields a surface concentration of about 33 μmol/m². The present treatment is restricted to the ideal case.

As is argued below and elsewhere,⁽¹⁾ the most important species with regard to the generation of cation vacancies is the absorbed aggressive ion, X_o^\bullet , and hence it is of interest to examine the absorption isotherm for this species in some detail. Substitution for the G-values in Equation (15) therefore yields

$$\Gamma_{X_o} = \frac{K_{II}^0 \Gamma^0 e^{(\alpha V + \beta p H) F / RT} a_X}{1 + K_I^0 e^{2(\alpha V + \beta p H) F / RT} a_{H^+}^2 + K_{II}^0 e^{(\alpha V + \beta p H) F / RT} a_X + K_{III}^0 e^{z(\alpha V + \beta p H) F / RT} a_Y} \quad (20)$$

This equation has a number of important limiting forms:

1. Inhibitor Absent. In this case, $a_Y = 0$ and Equation (20) reduces to

$$\Gamma_{X_o} = \frac{K_{II}^0 \Gamma^0 e^{(\alpha V + \beta p H) F / RT} a_X}{1 + K_I^0 e^{2(\alpha V + \beta p H) F / RT} a_{H^+}^2 + K_{II}^0 e^{(\alpha V + \beta p H) F / RT} a_X} \quad (21)$$

Noting that G_I is of the order of G_{II}^2 , it is reasonable to assume that oxygen ions are more strongly absorbed into oxygen vacancies than is the aggressive anion, X^- , so that Equation (21) further reduces to

$$\Gamma_{X_o} = \frac{K_{II}^0 \Gamma^0 e^{(\alpha V + \beta pH)F/RT}}{1 + K_I^0 e^{2(\alpha V + \beta pH)F/RT} a_{H^+}^2} a_X \quad (22)$$

This relationship predicts that the concentration of absorbed aggressive anion is linearly related to the activity of the anion in the solution. This is postulated to be the “normal” aggressive ion-induced breakdown case, because we will see below that the correct relationship is predicted between the critical breakdown potential and the ion activity.

In the limit of very strong adsorption, where the third term dominates the denominator of Equation (21), $\Gamma_{X_o} \approx \Gamma^0$ and the concentration of adsorbed X^- on the surface becomes independent of the activity of the ion in the solution. In this case, essentially every surface oxide ion is replaced by X^- and the outer surface corresponds to a “salt film”. Given the high stabilities of oxides versus halides, it is unlikely that this limit is approached in practice.

2. Inhibitor Present. In this instance, $a_Y > 0$, and Equation (20) shows that, in all cases, the absorption of Y^{z-} acts to inhibit the generation of X_o^\bullet . If the absorption of Y^{z-} is sufficiently strong, the concentration of X_o^\bullet takes the form

$$\Gamma_{X_o} = \Gamma^0 \frac{K_{II}^0 e^{(\alpha V + \beta pH)F/RT}}{K_{III}^0 e^{z(\alpha V + \beta pH)F/RT}} \left(\frac{a_X}{a_Y} \right) \quad (23)$$

In this important case, the concentration of the absorbed X^- , X_o^\bullet , is determined not only by the voltage and pH, but also by the ratio of the activities of X^- and Y^{z-} in the system. For the very special case, where $z = 1$, Equation (23) is reduced to the even simpler form

$$\Gamma_{X_o} = \Gamma^0 \frac{K_{II}^0}{K_{III}^0} \left(\frac{a_X}{a_Y} \right) \quad (24)$$

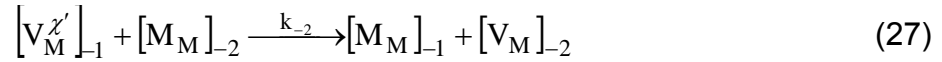
in which the voltage- and pH-dependencies are lost. These are important diagnostic criteria that should be amenable to direct experimental evaluation.

Cation Vacancy Generation

The theory for passivity breakdown inhibition developed in this work postulates that species X_O^\bullet , which may be written in more illustrative form as $(M_M)_p X_O^\bullet$, in order to recognize that there exists one or more (p) neighboring surface cations, undergoes a suitable fluctuation, such that cation extraction occurs (Figure 4) to produce a cation vacancy/oxygen vacancy pair in the surface of the barrier layer, $(M_M)_{p-1} V_M V_O^{(2-\chi)\bullet}$, and to regenerate the aggressive ion, X^-



Subsequently, the vacancy pair is annihilated by the transfer of a cation from the juxtaposition cation layer below the surface in a process that regenerates the surface oxygen vacancy $[(M_M)_p V_O^{\bullet\bullet} \equiv V_O^{\bullet\bullet}]$ and leads to the formation of a subsurface cation vacancy, $[V_M^{\chi'}]_{-1}$. Subsequently, this vacancy is annihilated by movement of a cation from the next deepest cation layer, with the process being repeated until the cation vacancy is transferred to the metal/barrier layer interface as depicted in Figure 4. These process can be depicted by the reactions, in which $p = 1$ for simplicity



Using the steady-state hypothesis from chemical kinetics, and regarding $V_M V_O^{(2-\chi)\bullet}$ and $[V_M^{\chi'}]_{-1}$ as being intermediates, we obtain

$$\frac{d[(V_M^{\chi'})_{-1}]}{dt} = k_{-1} [V_M V_O^{(2-\chi)\bullet}] - k_{-2} [(V_M^{\chi'})_{-1}] = 0 \quad (28)$$

and

$$\frac{d[V_M V_O^{(2-\chi)\bullet}]}{dt} = k_0 I_{X_O} - k_{-1} [V_M V_O^{(2-\chi)\bullet}] = 0 \quad (29)$$

In deriving these equations, it is assumed that the concentration of cations on each layer remains constant and hence that the rate constants are pseudo first order. This assumption is judged to be valid, provided the vacancy population on the cation sublattice is no more than a few percent. In any event, the theory is readily extended to the more exact treatment, in which the cation concentrations are included as variables, albeit at a significant cost in mathematical complexity.

Equations (28) and (29) therefore yield

$$\left[(V_M^{\chi'})_{-1} \right] = \frac{k_{-1}}{k_{-2}} \left[V_M V_O^{(2-\chi)\bullet} \right] \quad (30)$$

and

$$\left[V_M V_O^{(2-\chi)\bullet} \right] = \frac{k_0}{k_{-1}} \Gamma_{X_0} \quad (31)$$

and hence

$$\left[(V_M^{\chi'})_{-1} \right] = \frac{k_0}{k_{-2}} \Gamma_{X_0} \quad (32)$$

The flux of cation vacancies from the barrier layer/solution interface to the metal/barrier layer interface can be expressed in terms of the Nernst-Planck equation as

$$J_{CA} = -D \frac{\partial C_V}{\partial x} + \chi \gamma D \varepsilon C_V \quad (33)$$

where D is the cation vacancy diffusivity, ε is the electric field strength, $\gamma = F/RT$, and $C_V \equiv \left[(V_M^{\chi'})_{-1} \right]$. Note that, in the PDM, the electric field strength is assumed to be constant (independent of the applied voltage and of the distance through the film); the former because of buffering by Esaki tunneling¹ and the latter for mathematical simplicity. It is further assumed that the flux is driven primarily by the electric field and hence that

$$J_{CA} \approx \chi \gamma D \varepsilon C_V = \chi \gamma D \varepsilon \frac{k_0}{k_{-2}} \Gamma_{X_0} \quad (34)$$

where the surface concentration of aggressive ions adsorbed into oxygen vacancies is given in the general case by Equation (20).

In order to evaluate J_{CA} from Equation (34), it is necessary to expand k_0 and k_{-2} as functions of more fundamental parameters. This can be done using the Method of Partial Charge Transfer¹² to yield

$$k_{-2} = k_{-2}^0 e^{\chi \alpha_{-2} \varepsilon \gamma d} \quad (35)$$

and

$$k_0 = k_0^0 e^{\alpha_0 \alpha (\delta-1) \gamma V} e^{\alpha_0 \beta (\delta-1) \gamma pH} \quad (36)$$

where $\gamma = F/RT$, α_{-2} and α_0 are transfer coefficients, α is the polarizability of the film/solution interface, β is the dependence of the potential drop across the film/solution interface on the pH, V is the applied voltage, and d is the spacing between cation layers in the barrier layer of the passive film. Substitution of Equations (35) and (36) into Equation (34), and then by recognizing that the critical breakdown potential is given by the condition that $J_{CA} = J_m$, where J_m is the rate of vacancy annihilation at the metal/film interface, the critical breakdown potential is given by:

$$V_c = \frac{2.303RT}{\alpha[1-z+\alpha_0(\delta-1)]F} \ln\left(\frac{J_m K_{III}^0 k_{-2}^0 e^{\alpha_{-2}\chi\epsilon\gamma d}}{\chi\epsilon\gamma D k_0^0 K_{II}^0 \Gamma^0}\right) - \frac{\beta}{\alpha} \text{pH} - \frac{2.303RT}{\alpha[1-z+\alpha_0(\delta-1)]F} \log\left(\frac{[X^-]}{[Y^{z-}]}\right) \quad (37)$$

The reader will note that Equation (37) has the form of the experimentally derived Equation (1); that is, the extent to which an oxyanion (Y^{z-}) can inhibit passivity breakdown due to the aggressive anion, X^- , depends upon the ratio of the concentrations. It should be noted that Equation (37) was derived assuming strong adsorption of the inhibitor, Y^{z-} . Other conditions (e.g., weak adsorption) produce other expressions; these will be presented in later papers from this program and will be evaluated as the requisite data become available.

Examination of Equation (37), and recognizing that z and δ are commonly 1 and 2, respectively, the relationship between the critical breakdown potential and the ratio of the concentrations of X^- and Y^{z-} becomes

$$V_c = \frac{2.303RT}{\alpha\alpha_0 F} \ln\left(\frac{J_m K_{III}^0 k_{-2}^0 e^{\alpha_{-2}\chi\epsilon\gamma d}}{\chi\epsilon\gamma D k_0^0 K_{II}^0 \Gamma^0}\right) - \frac{\beta}{\alpha} \text{pH} - \frac{2.303RT}{\alpha\alpha_0 F} \log\left(\frac{[X^-]}{[Y^{z-}]}\right) \quad (38)$$

Thus, by measuring the critical breakdown potential, V_c , as a function of $\log\left(\frac{[X^-]}{[Y^{z-}]}\right)$, it is possible to determine the product $\alpha\alpha_0$. However, as described in Ref. (2), α is readily determined by plotting V_c against $\log\left(\frac{[X^-]}{[Y^{z-}]}\right)$, so that α_0 may be determined unequivocally.

Finally, development of the expression for the induction time for an individual pit² and extension of the above theory to Damage Function Analysis^{1,9} is straight forward and will be reported later. Completion of this task will essentially provide a deterministic theory that is capable of accounting for, on a quantitative basis, the impact of inhibiting anions on the accumulation of localized corrosion damage

COMPARISON WITH EXPERIMENT

Dependence of Breakdown Voltage on System Composition

Extensive experimental work has been carried out in this laboratory on the inhibition of chloride ion passivity breakdown on Type 316 SS by nitrate ion in borate buffer solution. The details of the experimental work is given elsewhere,¹³ so that only a summary is given here. Briefly, the experiments were performed in NaCl solution

containing various amounts of NaNO₃. Unless specified, the solutions contain 0.200 M H₃BO₃ adjusted to pH = 8.50±0.05 by adding NaOH. Before each experiment, the solution was sparged with 99.995% N₂ gas for 2 hours. During an experiment, the gas flow rate was reduced to one bubble every 2-3 seconds, in order to maintain deaerated conditions. A 5-minute cathodic stripping treatment of the working electrode was performed to activate the surface, followed by a waiting period of 30 minutes. Subsequently, a potentiodynamic scan was initiated from -0.7 V_{SCE} to 1.3 V_{SCE} unless the current reached 1.0 mA, in which case the scan was terminated.

Figure 5 shows the influence of the borate buffer solution on the critical breakdown potential. The critical potential rises with increasing [H₃BO₃], with the empirical relationship being given as

$$V_c = 0.305 + 0.101 * \log[H_3BO_3] \quad (39)$$

indicating that the buffer itself is an inhibitor of passivity breakdown on Type 316 SS in chloride-containing solutions. The reproducibility was found to be best when the boric acid concentration was about 0.20 M, so that all of the experiments described below employed 0.20 M H₃BO₃ + NaOH. Now, Equation (37) can be rewritten as

$$V_c = V_0 - \frac{\beta}{\alpha} \text{pH} - \frac{2.303RT}{\alpha F} \log[Cl^-] \quad (40)$$

where α is the polarizability of the film/solution interface and β is the dependence of the potential drop across the barrier layer/solution interface on pH; both can be determined by measuring V_c at different pH values and chloride concentrations. Thus, Figure 6 shows the critical potential versus chloride ion concentration correlation, while Figure 7 displays the critical potential at different pH values. Parenthetically, it is noted that the critical potential measurements became more reproducible at higher chloride concentration. Using these data, the critical breakdown potential as a function of [Cl⁻] and pH can be described by the following equations:

$$V_c = 0.140 - 0.175 * \log[Cl^-] \quad (41)$$

and

$$V_c = -0.266 + 0.060 * \text{pH} \quad (42)$$

Based on Equations 41 and 42, α is determined to be 0.338 and β is calculated to be -0.020 V, which is comparable to the previously reported values.⁵ The V_0 values [Equation (40)] are calculated to be -0.388 V and -0.370 V_{SCE} from Equations (41) and (42), respectively. The excellent agreement of the values for V_0 determined from the two sources demonstrates the viability of the PDM for describing passivity breakdown on Type 316L SS in chloride-containing solutions.

Potential Scan Rate Dependence of the Critical Breakdown Potential

Figure 8 shows the critical breakdown potential as a function of the potential scan rate. The breakdown potential, V_c , increases linearly with $v^{1/2}$, which has been observed previously by Haruna and Macdonald¹⁴ for nickel, Fonseca et al¹⁵ for aluminum, Zhang¹⁶ for Type 403 SS, and by Zhang and Macdonald¹⁷ for the same alloy, among others,¹⁸ and is predicted by the Point Defect Model.¹⁴ The theoretical relationship between V_c and $v^{1/2}$ can be described by the following equation:

$$V_c = 0.198 + 1.71 * v^{1/2} \quad (43)$$

where v is in units of V/s. For $v = 0.5$ mV/s, the average breakdown potential is 0.236 V_{SCE} , which is 0.038 V higher than the breakdown potential at zero scan rate; more importantly, perhaps, is the observation by Haruna and Macdonald¹⁴ and Zhang and Macdonald¹⁷ that the gradient of V_c versus $v^{1/2}$ is essentially independent of the concentration of the aggressive species. Due to the intrinsic uncertainty in the measured V_c (± 0.05 V, note that the breakdown voltage is a distributed parameter reflecting an underlying distribution in the breakdown sites with regard to the cation vacancy diffusivity,^{1,19,20} it is probably justified to use the measured V_c at a finite voltage sweep rate of, say, 0.5 mV/s as a practical way of minimizing the number of experiments that must be performed. In any event, the measured breakdown voltage may be corrected to zero scan rate as described below.

According to the PDM,¹⁴ V_c is related to the potential scan rate as:

$$V_c(v) = \left(\frac{2\xi RT}{J_m \chi F \alpha} \right)^{1/2} v^{1/2} + V_c(v=0) \quad (44)$$

Employing the value of α determined earlier, the value of ξ , which is the critical areal (two-dimensional) concentration of condensed vacancies at the metal/barrier layer interface, can be determined. The quantity J_m , which is the rate of annihilation of cation vacancies at the metal/barrier layer interface, should be, at most, the value of the flux of cation vacancies moving through the passive film from barrier layer/solution interface to metal/barrier layer interface (J_{ca}). However, for a cation vacancy-conducting film (e.g., passive Ni,²¹ J_{ca} may be calculated from the measured passive current at the point of breakdown (I_{ss}^{bd}) as

$$J_{ca} = \frac{I_{ss}^{bd} N_{AV}}{\chi F} \quad (45)$$

where N_{AV} is the Avogadro's number and $\chi = 3$, because the passive film is assumed to be defective Cr_2O_3 . The value of I_{ss}^{bd} was found to be approximately 2 $\mu A/cm^2$, J_{ca} is estimated to be $4.1 \times 10^{12} cm^{-2} s^{-1}$, and J_m is at least $4.1 \times 10^{12} cm^{-2} s^{-1}$. The value of the areal (two-dimensional) concentration of condensed cation vacancies, ξ , is therefore at

least $2.4 \times 10^{14} \text{ cm}^{-2}$. Because the concentrations of cations in the oxide and of metal atoms in the alloy are related to the structures of Cr_2O_3 and the substrate steel, respectively, we can estimate the values of ξ for vacancy condensation on the cation sublattice of the barrier layer on the film side of the interface or on the metal lattice on the substrate side of the boundary. Because the barrier layer on stainless steels comprise defective chromic oxide, $\text{Cr}_{1+x}\text{O}_{1-y}$, recognizing that the layer is n-type in electronic character and hence that the principal point defect must be the cation interstitial ($x > 0$) or oxygen vacancy ($y > 0$), or both ($x, y > 0$), we assume that the metal substrate on the metal side of the interface corresponds to chromium metal. Based on the available structural information, the areal atomic density for Cr and Cr_2O_3 is $1.2 \times 10^{15} \text{ cm}^{-2}$ and $4.0 \times 10^{14} \text{ cm}^{-2}$, respectively.¹⁶ This level of agreement is typical of that observed in other systems¹⁴⁻¹⁷ and provides powerful confirmation of the validity of the Point Defect Model for describing passivity breakdown.

Oxyanion Inhibition of Passivity Breakdown

Oxyanion inhibition of passivity breakdown on Type 316L SS was explored in solutions of $\text{NaCl} + \text{NaNO}_3$ with borate as the buffering agent. Figure. 9 shows measured critical potential versus $\log[\text{Cl}^-]$ for solutions with and without nitrate ion. The linear dependencies are consistent with Equations (37) and (38) as predicted by the PDM and the fact that the correlations are parallel signifies that the value of α is the same for the two cases. Thus, V_c is predicted to decrease linearly with $\log\left(\frac{[\text{Cl}^-]}{[\text{NO}_3^-]}\right)$ as:

$$V_c = \frac{2.303RT}{\alpha\alpha_0F} \ln\left(\frac{J_m K_{\text{III}}^0 k_{-2}^0 e^{\alpha_2 \chi \varepsilon \gamma d}}{\chi \varepsilon \gamma D k_0^0 K_{\text{II}}^0 \Gamma^0}\right) - \frac{\beta}{\alpha} \text{pH} - \frac{2.303RT}{\alpha\alpha_0F} \log\left(\frac{[\text{Cl}^-]}{[\text{NO}_3^-]}\right) \quad (46)$$

The experimental results can be summarized in similar form as:

$$V_c = 0.543 - 0.176 * \log\left(\frac{[\text{Cl}^-]}{[\text{NO}_3^-]}\right) \quad (47)$$

where α_0 is calculated to be 0.994. The reader will recall that α_0 is the transfer coefficient for the cation ejection reaction (Figure 4, fourth reaction from the top) and a value of one signifies a strong potential dependence. Thus, ejection of the cation from the barrier layer to form $(M_M)_{p-1}(V_M V_O)^{(2-\chi)\bullet}$ at the barrier layer/solution interface is a charge transfer process, presumably leading to the formation of Cr(IV) or Cr(VI) in the solution. If the latter is the case, the process might be labeled “chloride catalyzed, localized transpassive dissolution” in recognition of the fact that transpassive dissolution appears to coincide with the electrochemically mediated ejection of chromate [Cr(VI)] from the surface and concomitant oxidative dissolution of the barrier layer.²²

With the chloride concentration fixed at 0.30 M, the critical breakdown potential was measured as a function of the concentration of nitrate, as shown in Figure 10. The

critical breakdown potential increases slightly with increasing nitrate concentration at low $[\text{NO}_3^-]$, while at higher concentration, the pitting potential rises very quickly and no pitting is observed when $[\text{NO}_3^-]$ is above 0.060 M. A similar result for Type 316 SS has also been reported by Dahan.²³ We interpret the sudden increase in V_c as indicating saturation of the surface oxygen vacancy absorption sites at the barrier layer/solution interface, such that chloride ion are excluded, at least at those sites at which breakdown occurs.

The final issue that we wish to discuss is: Why do not the oxyanions themselves induce passivity breakdown in a manner that parallels that for chloride ion? After all, it is postulated that the oxyanions absorb into surface oxygen vacancies, so that they might also be expected to catalyze cation ejection and generate an enhanced flux of cation vacancies across the barrier oxide layer, ultimately leading to passivity breakdown. We do not have a clear answer to this question at this time, other than to postulate that oxyanion absorption is irreversible and hence cannot aid in cation extraction.

SUMMARY AND CONCLUSIONS

A theory has been developed within the framework of the Point Defect Model (PDM) for the inhibition of passivity breakdown by oxyanions in solution. Inhibition is attributed to competitive adsorption of the oxyanions into surface oxygen vacancies in a manner that does not result in cation vacancy generation, thereby depriving chloride ion from absorption sites at the barrier layer/solution interface. The theory yields the correct dependence of the breakdown voltage on the ratio of the concentrations of the aggressive anion and the inhibitor. Measurement of the critical breakdown potential (V_c) as a function of the voltage sweep rate (v) in potentiodynamic scans shows that V_c varies linearly with $v^{1/2}$, in accordance with the prediction of the PDM. This relationship permits calculation of the areal (two-dimensional) concentration of vacancies in the vacancy condensate that is envisioned to form at the metal/barrier layer interface and to be responsible for passivity breakdown. The concentration obtained is found to be in good agreement with values calculated from structural arguments assuming condensation on the cation sub-lattice of the film or on the metal lattice, thereby providing powerful evidence for the viability of the PDM for describing passivity breakdown.

ACKNOWLEDGEMENTS

Support by the Science & Technology Program of the Office of the Chief Scientist (OCS), Office of Civilian Radioactive Waste Management (OCRWM), U.S. Department of Energy (DOE), is gratefully acknowledged. The work was performed under the Corrosion and Materials Performance Cooperative, DOE Cooperative Agreement Number: DE-FC28-04RW12252. The views, opinions, findings, and conclusions or recommendations of authors expressed herein do not necessarily state or reflect those of the DOE/OCRWM/OCS. Finally, we gratefully thank Penn Stainless Products for

providing the stainless steel samples. We also acknowledge fruitful discussions with Dr. George Engelhardt and with Dr. Yancheng Zhang.

REFERENCES

1. D. D. Macdonald, *Pure Appl. Chem.*, 51, (1999): p.971.
2. L. F. Lin, C. Y. Chao, and D. D. Macdonald, *J. Electrochem. Soc.*, 128, (1981): p.1194.
3. H. H. Strehblow and B. Titze, *Corros. Sci.*, 17, (1977): p.461.
4. E. McCafferty, *J. Electrochem. Soc.*, 137, (1990): p.3731.
5. C. Lemaitre, B. Baroux, and G. Beranger, *Key Eng.Mat.*, 20-28, (1987): p.2841.
6. C. Lemaitre, B. Baroux, and G. Beranger, *Werkst. Korr.*, 40, (1989): p.229.
7. V. S. Muralidharan, *Corros. Rev.*, 21, (2003): p.327.
8. S. B. Basame and H. S. White, *J. Electrochem. Soc.*, 147, (2000): p.1376.
9. G. R. Engelhardt and D. D. Macdonald, *Corrosion*, 54, (1998): p.469.
10. C. B. Bargeron and R. B. Givens, *J. Electrochem. Soc.*, 124, (1977): p.1845.
11. C. B. Bargeron and R. B. Givens, *Corrosion*, 36, (1980): p.618.
12. D. D. Macdonald, unpublished findings (1985).
13. S. Yang and D. D. Macdonald, *Electrochim. Acta*, in press (2006).
14. T. Haruna and D. D. Macdonald, *J. Electrochem. Soc.*, 144, (1997): p.1574.
15. I. T. E. Fonseca, N. Lima, J. A. Rodrigues, M. I. S. Pereira, J. C. S. Salvador, and M. G. S. Ferreira, *Electrochem. Comm.*, 4, (2002): p.353.
16. Y. Zhang, PhD Thesis, Penn State University, 2005.
17. Y. Zhang, D. D. Macdonald, M. Urquidi-Macdonald, G. Engelhardt, and R. B. Dooley, *Corros. Sci.*, in press (2006).
18. S. Szklarska-Smialowska, *Pitting Corrosion of Metals*, NACE, Houston, TX, 1986.
19. D. D. Macdonald and M. Urquidi-Macdonald, *Electro. Acta.*, 31, (1986): p1079.
20. D. D. Macdonald and M. Urquidi-Macdonald, *J. Electrochem. Soc.*, 137, (1990): p.2395.
21. E. Sikora and D. D. Macdonald, *Electrochim. Acta*, 48, (2002): p.69.
22. D. D. Macdonald, *J. Electrochem. Soc.*, 153, (2006): p.B213.
23. H. A El Dahan, *J. Materials Sci.*, 34, (1999): p.851.

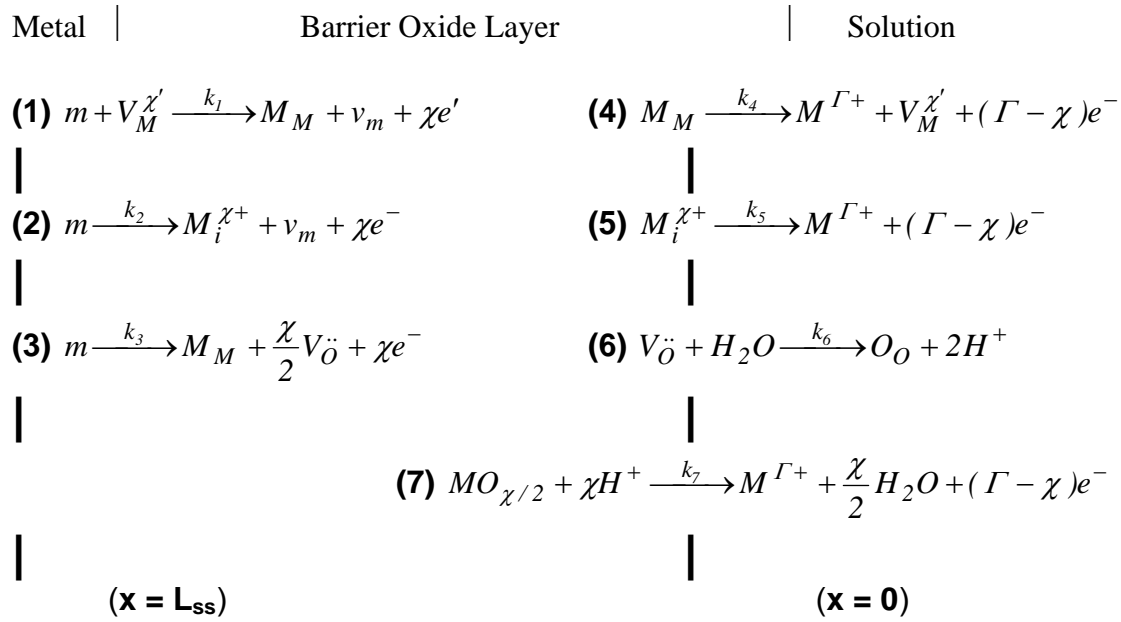


Figure 1. Interfacial defect generation/annihilation reactions that are postulated to occur in the growth of anodic barrier oxide films according to the Point Defect Model.⁴ m = metal atom, $V_M^{\chi'}$ = cation vacancy on the metal sublattice of the barrier layer, $M_i^{\chi+}$ = interstitial cation, M_M = metal cation on the metal sublattice of the barrier layer, $V_O^{\bullet\bullet}$ = oxygen vacancy on the oxygen sublattice of the barrier layer, O_O = oxygen anion on the oxygen sublattice of the barrier layer, $M^{\Gamma+}$ = metal cation in solution.

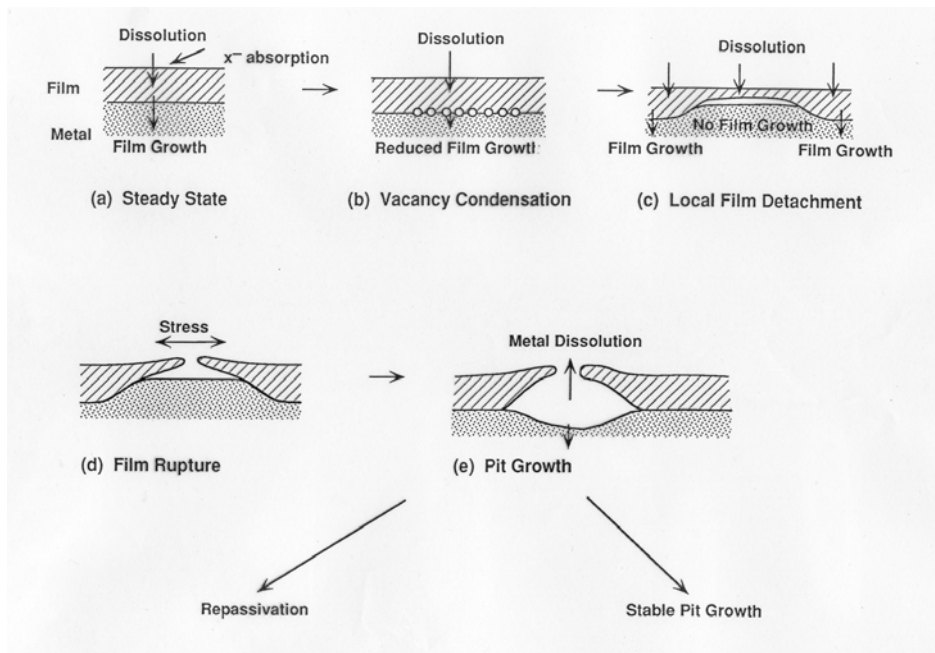


Figure 2. Schematic of the passivity breakdown process, as envisioned by the Point Defect Model.¹ The key concept is that a necessary condition for passivity breakdown is that the growth of the barrier layer into the substrate must be prevented; this is achieved in the PDM by cation vacancy condensation, which effectively separates the film from the metal while allowing for continued dissolution of the barrier layer at the barrier layer/solution interface. Note also, that cation vacancy condensation can only occur where the barrier layer is still connected to the metal, and hence the preferred site of cation vacancy condensation is at the periphery of the blister, resulting in the growth of the blister until breakdown occurs. The size of the blister is determined by competition between the rate of expansion of the blister by cation vacancy condensation and the dissolution of the barrier layer above the breakdown site.

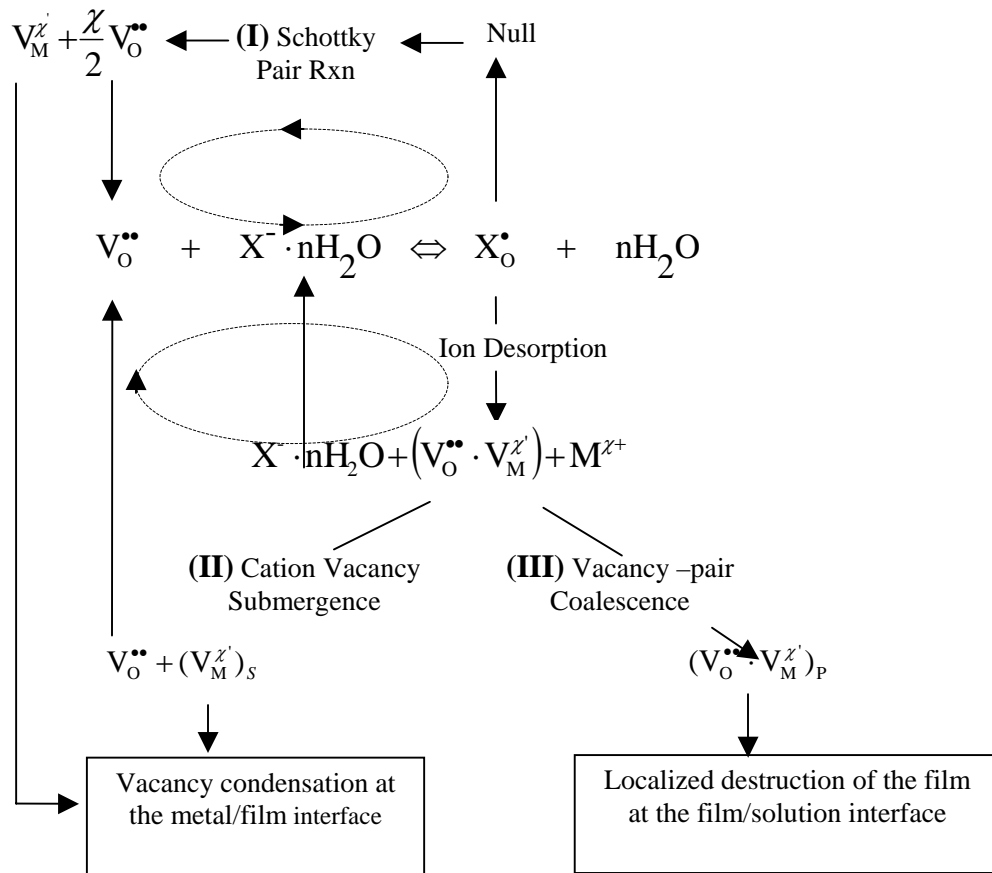


Figure 3. Possible mechanisms for the role of an aggressive anionic species (e.g., Cl^-) in passivity breakdown on passive metals and alloys.¹ Two catalytic processes are envisioned, as identified by the broken circulars. Both processes lead to the regeneration of oxygen vacancies and chloride ion, while also generating cation vacancies that are annihilated by the occupation of the sites by cations from within the film. These processes pump cation vacancies into the film, resulting in the condensation of cation vacancies at the metal/film interface, because the cation vacancy annihilation reaction at that location is incapable of accommodating the cation flux. Note also that these processes will occur at the periphery of the vacancy condensate, thereby explaining the observation of Barger and Givens^{10,11} that the absorbed chloride relocates to the edge of the blister (on aluminum) as the blister grows.

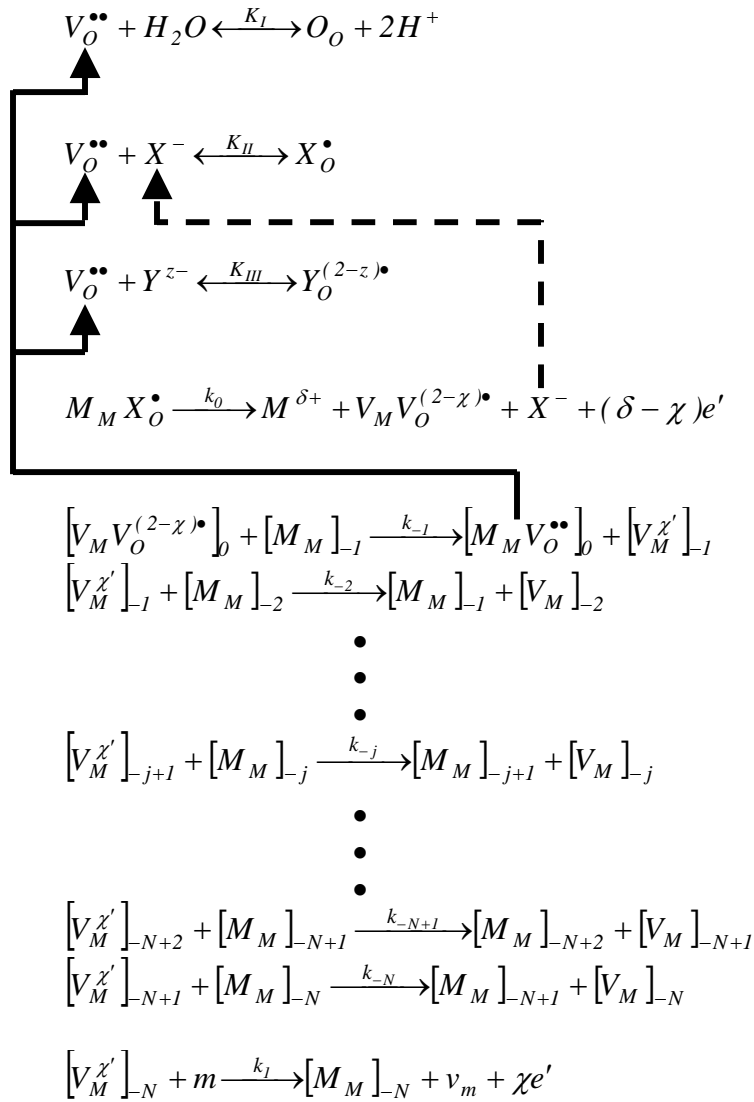


Figure 4. Reaction scheme for the autocatalytic generation of cation vacancies at the metal/barrier layer interface and of oxygen vacancies (solid lines) and aggressive anion X^- (broken lines) over the site on the surface where cation vacancy condensation and hence passivity breakdown occurs. Competitive absorption for the surface oxygen vacancies by water, X^- , and the inhibitor, Y^{z-} , is described by the first three reactions at the top of the figure. Note that the barrier layer is assumed to comprise N cation layers with the 0^{th} layer being located at the barrier layer/solution interface and the $-N^{\text{th}}$ layer adjacent to the metal/barrier layer interface. Cation vacancy condensation is assumed to occur upon the $-N^{\text{th}}$ cation layer. Note that the cation vacancy annihilation reaction corresponds to Reaction (1), Figure 1. m = metal atom, v_m = vacancy in the metal phase.

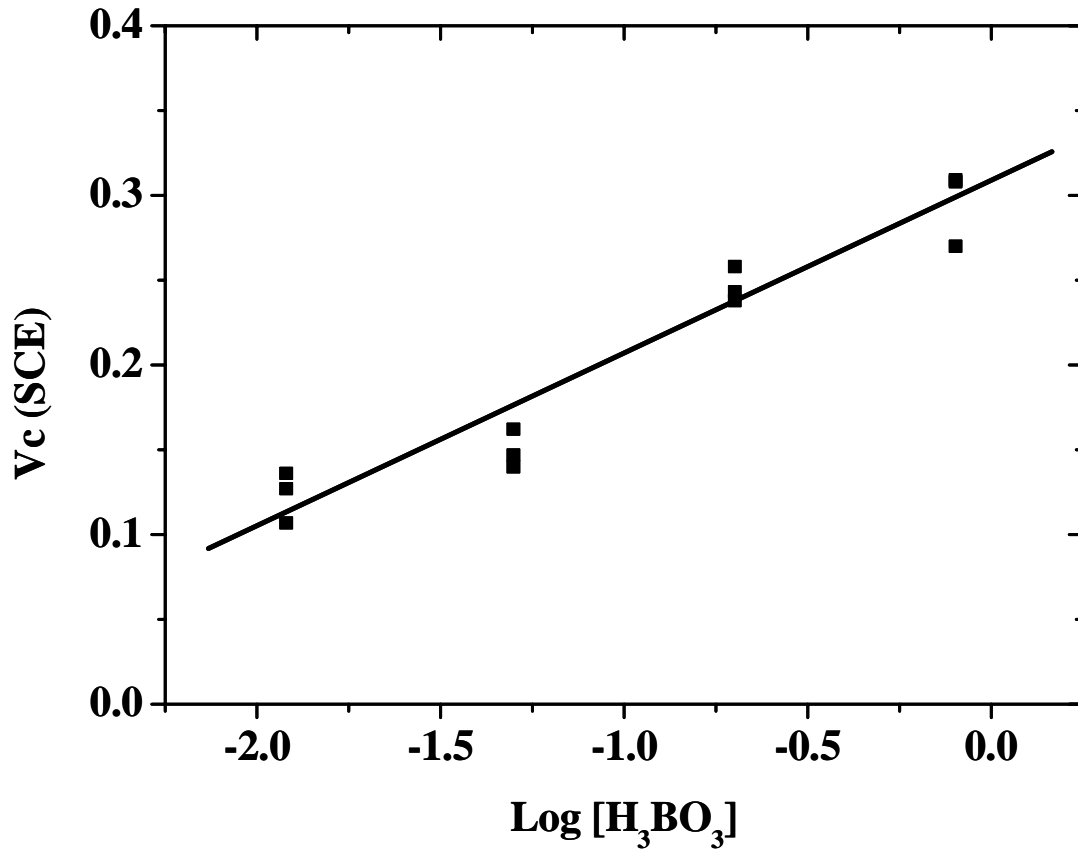


Figure 5. Critical breakdown potential for Type 316L SS in the presence of different amounts of boric acid at ambient temperature (22 ± 2 °C). $[\text{NaCl}] = 0.200$ M and voltage scan rate was 0.5 mV/s.¹³

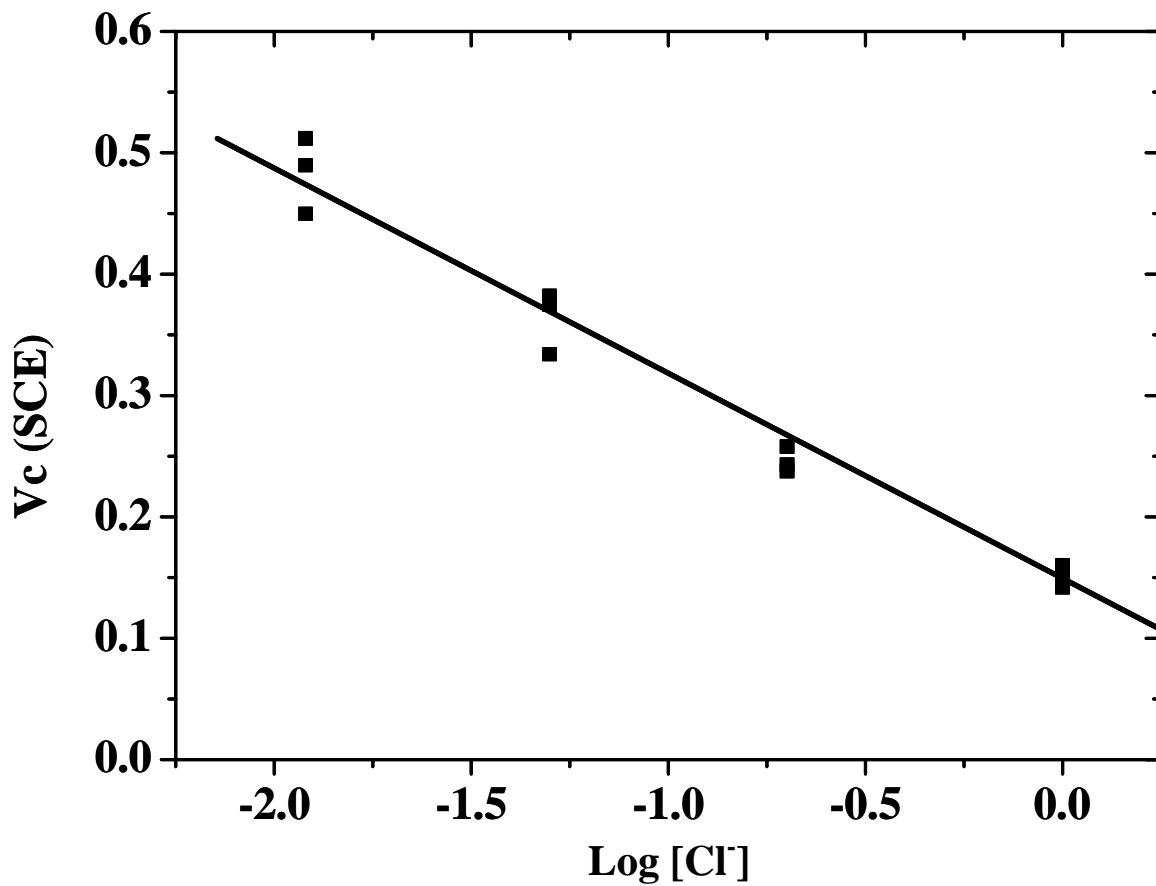


Figure 6. Critical breakdown potential for Type 316L SS as a function of chloride concentration at ambient temperature (22 ± 2 °C) and at pH = 8.50 ± 0.05 . The voltage scan rate was 0.5 mV/s.¹³

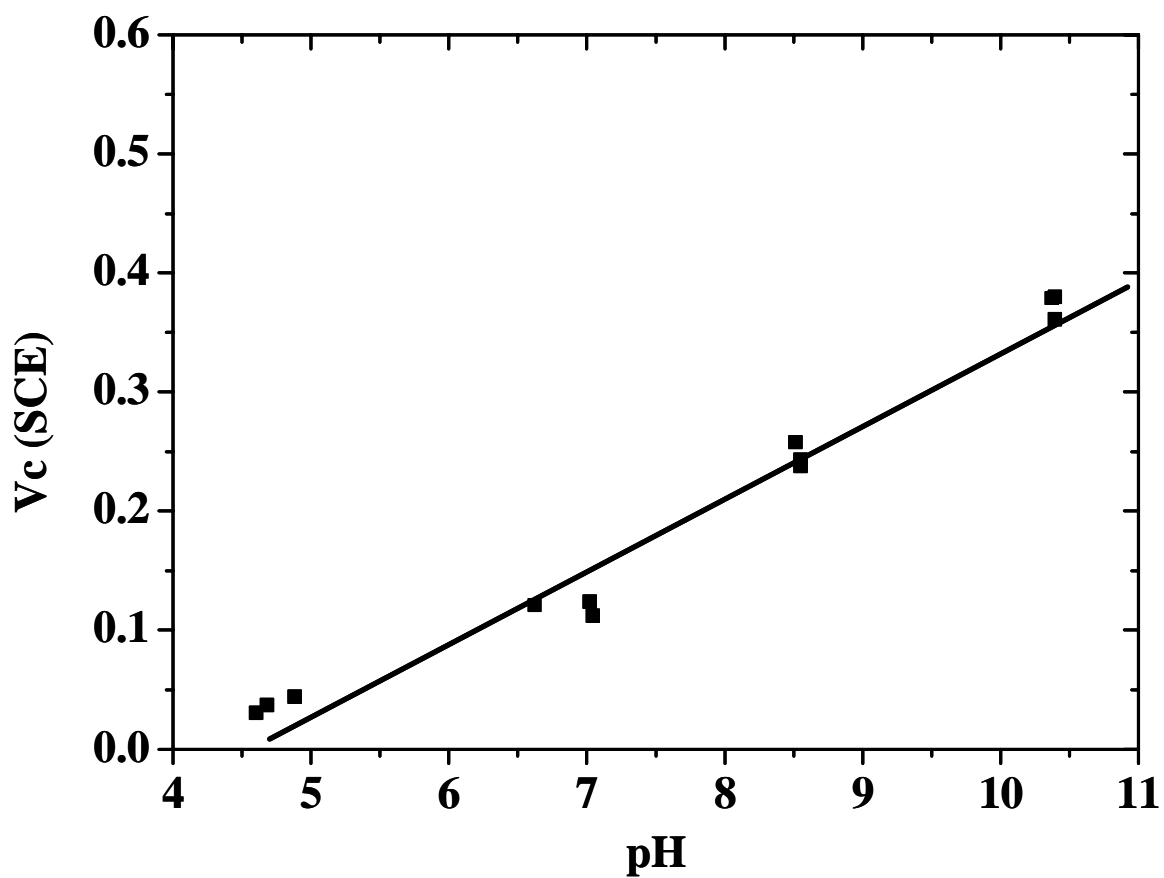


Figure 7. Critical breakdown potential for Type316L SS as a function of pH at ambient temperature (22 ± 2 °C). $[\text{NaCl}]$ and $[\text{H}_3\text{BO}_3]$ were both 0.20 M. The pH was adjusted by the addition of NaOH. Voltage scan rate = 0.5 mV/s.¹³

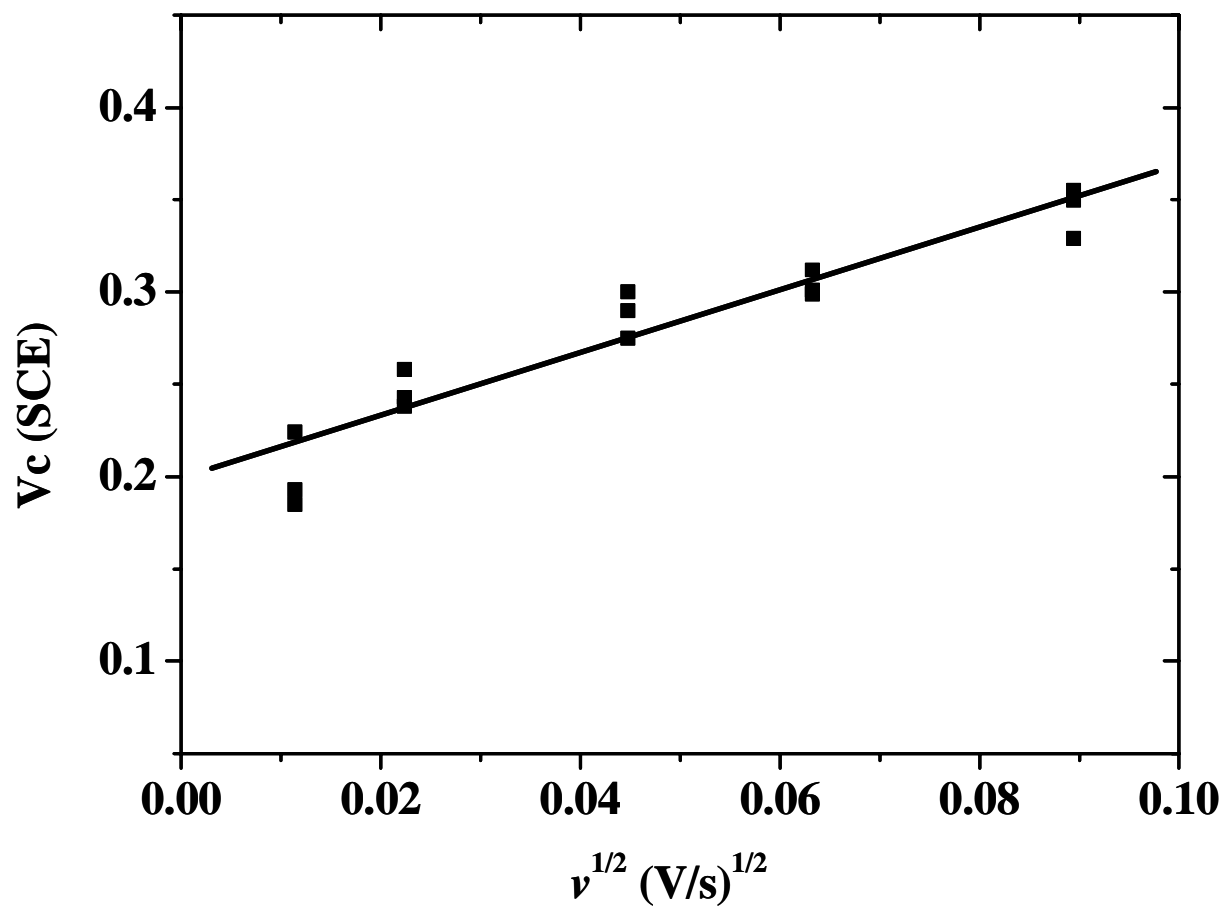


Figure. 8. Critical breakdown potential for Type 316 SS versus the square root of the potential scan rate at ambient temperature ($22 \pm 2 \text{ }^\circ\text{C}$). $[\text{NaCl}]$ and $[\text{H}_3\text{BO}_3]$ were both 0.20 M. Solution $\text{pH} = 8.50 \pm 0.05$.¹³

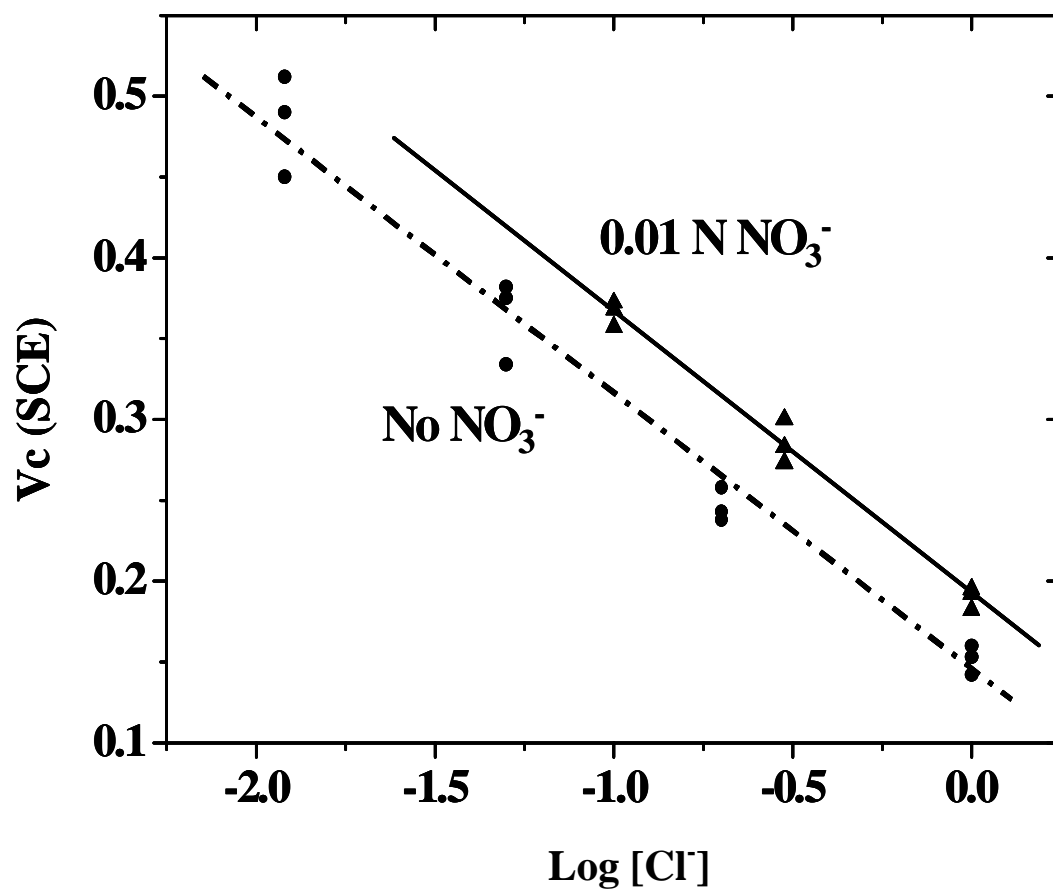


Figure 9. Critical breakdown potential for Type 316 SS in NaCl + borate buffer solution ($\text{pH} = 8.50 \pm 0.05$) with and without 0.01 N NO_3^- . The voltage scan rate was 0.5 mV/s .¹³

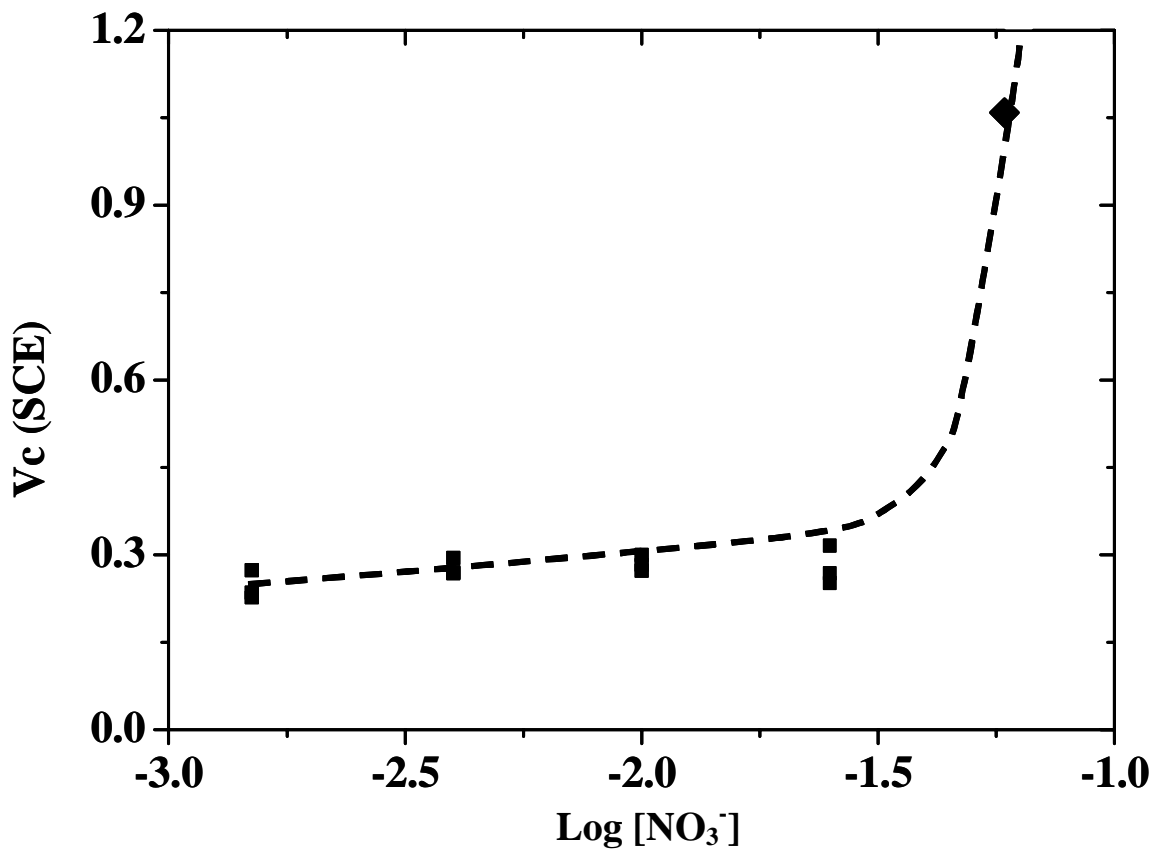


Figure 10. Critical breakdown potential for Type 316 SS as a function of nitrate concentration at ambient temperature (22 ± 2 °C) and at $\text{pH} = 8.50 \pm 0.05$. The voltage scan rate was 0.5 mV/s.¹³